In Situ Calorimetric, Structural, and Compositional Study of Zeolite Synthesis in the System $5.15Na_2O-1.00Al_2O_3-3.28SiO_2-165H_2O$

Sanyuan Yang and Alexandra Navrotsky*

Thermochemistry Facility, Department of Chemical Engineering and Materials Science, University of California at Davis, Davis, California 95616

Brian L. Phillips

Department of Chemical Engineering and Materials Science, University of California at Davis, Davis, California 95616

Received: December 17, 1999; In Final Form: March 29, 2000

The synthesis of FAU zeolite was studied in situ using scanning microcalorimetry at a slow heating rate of 0.10 °C/min. The scanning calorimetric heat flow (SCHF) curves showed characteristic exothermic peaks for both the precrystallization reactions and the crystallization. Combined with complementary characterization techniques, the structural and chemical changes in the zeolite synthesis system were identified and correlated with the SCHF peaks. Two mixtures of the same composition ($5.15Na_2O-1.00Al_2O_3-3.28SiO_2-165H_2O$) but prepared from different silica sources (colloidal silica vs silicate solution) for the syntheses of FAU zeolite were examined. A cyclic or oscillatory pattern for precrystallization reactions was observed for the first time. This precrystallization evolution pattern indicates the stepwise precrystallization reactions that may result in significant inhomogeneity of the Si/Al ratio in the microscopic domains of the amorphous precursor. The existence of the compositional inhomogeneity is consistent with the occurrence of the LTA zeolite impurity (Si/Al = 1.0) when colloidal silica is used but not when solution of dissolved silica is used. A small energetic driving force for the crystallization ($\Delta H = -2.1 \pm 0.1$ kJ/mol on TO_2 basis of the zeolite product) has been directly measured. The integral enthalpy change for the precrystallization reactions varies greatly depending on the nature of the starting materials. The implications of the thermodynamic results in zeolite synthesis are also discussed.

Introduction

In the synthesis of aluminosilicate zeolites, an amorphous gel is typically the first product of the interaction between aluminate and silicate or silica sol prior to the formation of any crystalline phases.[1−4] Even in highly diluted systems (so-called clear solutions), suspensions of nanometer-sized gel particles were detected as intermediate phases.[5,6] A similar evolution sequence occurs in the synthesis of other important materials such as aluminophosphate-based microporous molecular sieves.[4] This evolution pattern has been explained by the Ostwald step rule of successive reactions: the intermediate short-range-ordered amorphous phase is thermodynamically metastable but kinetically more accessible relative to the long-range-ordered crystalline phases.[1−4] However, neither the magnitude of the relative thermodynamic metastability nor the nature of the kinetic barrier of the self-assembly process of the long-range-ordered structures is well understood.

Observations from extensive synthesis studies indicate that the precrystallization history and the nature of the short-range-ordered intermediate phase often have significant bearing on the synthesis products.[1−4] For example, room-temperature aging of the initial mixtures for the synthesis of faujasite can significantly accelerate the crystallization and eliminate the formation of impurity phases.[1,2,7] An understanding of the complex series of physicochemical events that occur in zeolite synthesis is desired for achieving better control of synthesis. Difficulties in such an endeavor arise from the complexity of the heterogeneous synthesis mixture.[3] This is particularly true for the precrystallization period in which the solid phases are not only structurally amorphous but also compositionally heterogeneous.

The absorption or release of heat during the course of zeolite synthesis, as like in all other chemical phenomena, is associated with the breaking and making of chemical bonds. Calorimetry provides a reliable and direct way to link the microscopic chemical events at a molecular scale to a macroscopically measurable property. The integral heat is related to the overall enthalpy change of the system.[8,9] For slow processes, measurement of the dependence of the heat flow rate on time allows kinetic investigations to be carried out.[9] The principal advantage of using calorimetric methods is that the system is not disturbed during the measurement and the thermokinetic study gives continuous recordings of the system's evolution. Heat effects can be seen clearly whether the process involves amorphous or crystalline materials. Petrova et al.[10] used a calorimeter under isothermal conditions for studying the zeolitization of glasses and observed exothermic heat effects for the wetting of glasses, glass hydration and dissolution, and crystallization of zeolites. Surprisingly, the potential of this technique for in situ characterization of the zeolite synthesis process has not been exploited.

Synthesis temperature affects both the number of crystals nucleated and the rate of crystal growth.[5,11,12] In practice, the initial mixture for zeolite synthesis is typically prepared at room temperature and then heated to a higher temperature to complete

* To whom correspondence should be addressed.

10.1021/jp9944278 CCC: $19.00
Published on Web 06/02/2000

the synthesis. The temperature change is often fast and uncontrolled, inducing a temperature gradient that increases the heterogeneity of the synthesis system. The impact of such temperature gradients on the precrystallization process, which is highly susceptible to temperature change,[11,12] may be significant but has not been systematically studied.

In this study we investigated the zeolite synthesis process under constantly increasing temperature utilizing the advanced temperature-controlling capability of a scanning microcalorimeter. The heating rate and the zeolite synthesis systems were chosen so that the desired zeolite formation process could be completed within the attainable temperature range while performing calorimetric measurement. One additional advantage of using a constantly increasing temperature for the zeolite synthesis is that the early (often fast) chemical reactions will take place at lower temperatures and the later (often slow) ones at higher temperatures so that all the reactions can proceed at relatively comparable rates. The objective of this study is 2-fold: (1) measurement of the heat flow when heating the selected synthesis systems and (2) identification of the nature of the chemical reactions associated with the observed SCHF peaks and the mechanistic implications. We report here the results of our investigation for the synthesis system of $5.15Na_2O-1.00Al_2O_3-3.28SiO_2-165H_2O$, which is in the range typical for synthesis of FAU zeolite and also close to that for synthesis of LTA zeolite,[1] two of the technologically most important zeolites.

Experimental Section

Synthesis. A synthesis mixture (mixture I) with a composition of $5.15Na_2O-1.00Al_2O_3-3.28SiO_2-165H_2O$ was prepared as follows: 1.30 g of NaOH (Fisher, $1.00Na_2O-1.05H_2O$) and 0.788 g of sodium aluminate (Alfa, $1.26Na_2O-1.00Al_2O_3-0.450H_2O$) were dissolved by stirring in 10.84 g of deionized water. Colloidal solica (2.07 g) (Ludox H-40, $0.013Na_2O-1.00SiO_2-5.01H_2O$) was added to this solution, and the mixture was stirred for 30 min. The fluid mixture appeared slightly cloudy, but no settling of any precipitate was observed. A portion of the mixture (7.50 g) was placed in a Teflon-lined stainless steel vessel for the calorimetric measurement. Vessels used for synthesis were pretreated in HF solution to eliminate any residues having seeding effects. After the preset time of heating, the mixture was quickly withdrawn from the calorimeter and the solid and liquid portions were separated by filtration and washing. The collected solid sample was then air-dried and equilibrated to ambient conditions.

A second mixture (mixture II) was prepared by mixing sodium hydroxide solution with colloidal silica. A viscous gel formed immediately upon mixing. This mixture was made from the same proportions of source materials as mixture I except that sodium aluminate was not added. The mixture was stirred for 5 min after mixing. Mixture II has a composition of $3.88Na_2O-3.28SiO_2-165H_2O$.

The third synthesis mixture (mixture III) has the same composition as mixture I but was prepared by first dissolving the colloidal silica in the sodium hydroxide solution prior to mixing with aluminate solution. In contrast to mixture I, a milky slurry was observed shortly after mixing.

Scanning Microcalorimetry. Using a commercial differential heat flow microcalorimeter (Setaram C-80), the heat effects in mixture I, II, and III were measured with a heating rate of 0.10 °C/min. A stainless steel vessel and Teflon liner identical to that used to contain the sample were used for containing the reference. The energy equivalent of the calorimetric signal was calibrated by using electrically generated heats. The performance of the instrument was checked by heating 7.5 g of water under the same scanning rate as that used for the samples. Agreement of the measured heat enthalpy within 1.0% with the published value[13] was obtained (Figure 1).

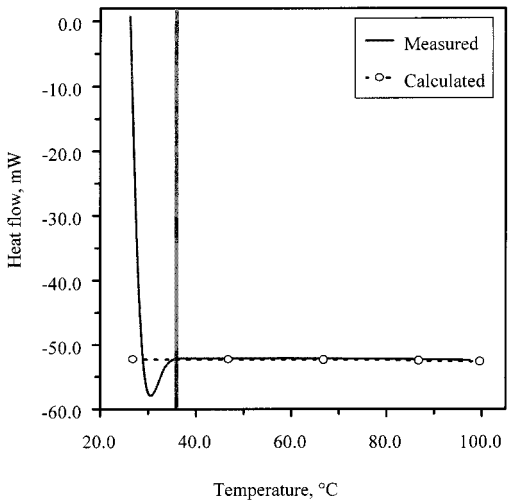

Figure 1. Comparison of the SCHF curve at 0.10 °C/min of 7.5 g of water measured and that calculated (based on C_p data from literature[13]). The initial part of the measured SCHF curve (left side of the bold line) corresponds to erratic signals prior to the attainment of a stable scanning mode.

The same amount of water (7.5 g) was used as the reference because its heat content is close to that of the synthesis system, which contains 82% water. This arrangement greatly reduced the baseline offset of the scanning calorimetric heat flow (SCHF) curve. To determine the heat effect of the system arising from chemical reactions, one has to eliminate the heat content contribution arising from heating the sample. This was done by correcting the measured SCHF curve (synthesis system versus water) with a baseline SCHF curve (Figure 2). The latter was obtained by repeating the calorimetric measurement of the same system (system-after-reaction versus water) after the synthesis was complete. The second heating of the system shows a contribution from the heat content but no measurable heat effects from chemical reactions as indicated by the flat SCHF curve (Figure 2).

The calorimetric data were calculated on the basis of the number of moles of TO_2 (T = Si, Al) of the final zeolite product as well as on the basis of the overall composition formula of the system. The TO_2 basis is convenient for evaluation of the crystallization. The overall composition formulas are convenient for evaluation of reactions that do not involve crystallization such as dissolution of silica. To keep internal consistency, the molar coefficients of Al_2O_3 in mixture I and mixture III were set to 1 and the coefficient of SiO_2 in mixture II was set the same as those in mixture I and mixture III.

Structural Studies. The ^{29}Si NMR spectra were taken with a Chemagnetics CMX-400 spectrometer operating at 79.5 MHz, with a sample probe configured for 7.5 mm rotors (outside diameter). For direct-polarization MAS (DP-MAS), the samples were spun at 5.0 kHz and the spectra acquired with 6 μs pulses ($\pi/2 = 8$ μs) separated by relaxation delays of 3−4 T_1's to yield quantitative intensity ratios. The T_1 for each resonance was estimated by the inversion−recovery null-point method and varied from 45 s for the amorphous silica phase to 20 s for the crystalline FAU phase, but these did not vary significantly among the different samples. Spectra for several samples taken with much longer relaxation delays did not show any significant

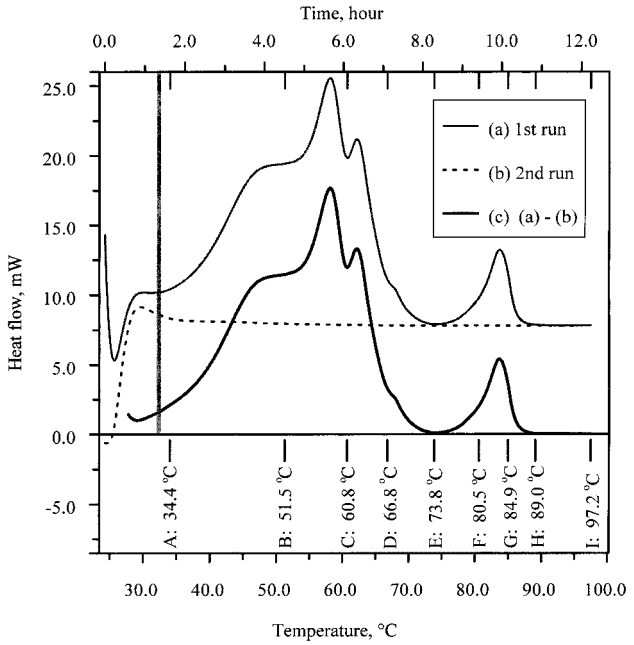

Figure 2. SCHF curves of mixture I ($5.15Na_2O-1.00Al_2O_3-3.28SiO_2-165H_2O$ at a constant linear heating rate of 0.10 °C/min. The same weight (7.50 g) of water was used in reference side. Repeated in situ experiments were performed and stopped at the selected temperatures denoted by capital letters.

differences. The $^{29}Si\{^1H\}$ CP-MAS spectra were acquired with a 3.6 kHz spinning rate and a ramp of the ^1H transverse field of approximately ±10 kHz about the match condition. For each resonance the ^1H $T_{1\rho}$ and $^{29}Si\{^1H\}$ cross-relaxation times (T_{IS}) were estimated from the variation in intensity with contact time (typically eight values from 0.1 to 20 ms). High-power ^1H decoupling was employed during all acquisitions. ^{23}Na and ^{27}Al MAS NMR spectra, taken at a 15 kHz spinning rate, contained only a single unresolved component at the expected chemical shifts and are not reported here.

Powder X-ray diffraction (XRD) patterns of the solid samples were measured on an Inel X-ray diffractometer (XRG 3000) using Ni-filtered Cu Kα radiation operated at 30 kV and 30 mA. The resolution of the position-sensitive detector is 0.029° 2θ. The radiation time of a sample is 50 min.

Chemical Analysis. Quantitative elemental analyses (of Na, Si, Al) were carried out by inductively coupled plasma emission spectroscopy (TJA Atomscan 25). Solid samples were dissolved in hot KOH solutions. Water content of the solid samples was determined from the weight loss after heating at 800 °C for 8 h. The results of the chemical analyses of the solid and liquid components are presented in Table 1 and Table 2, respectively.

Results and Discussion

In Situ Synthesis Using Colloidal Silica as Si Source (Mixture I: $5.15Na_2O-1.00Al_2O_3-3.28SiO_2-165H_2O$). *Scanning Microcalorimetry.* The SCHF curve of mixture I versus water at a heating rate of 0.10 °C/min from room temperature to 97.2 °C is presented in Figure 2 (curve a). The erratic signals seen in the early part of the curve (before 34 °C) are due to the initial instability of the calorimeter prior to the establishment of a stable scanning mode. After this period, several overlapping exothermic peaks were observed in the low-temperature range: one plateau or shoulder around 51.5 °C, one large peak between 51.5 and 60.8 °C, one small peak between 60.8 and 66.8 °C, and one very small shoulder between 66.8 and 73.8 °C. In the high-temperature range (73.8−89.0 °C), only one exothermic peak was seen. The SCHF curve flattens above 89.0 °C, indicating that any heat effects corresponding to further reactions are negligible. The exothermic baseline offset from zero heat flow is mainly attributed to the lower heat content of the mixture I system relative to an equal mass of water as a reference.

When the aqueous synthesis system was heated in the temperature range from 25 to 98 °C, the heat effect associated with vaporization within a closed vessel (dead volume ~ 1.0 mL) and the enthalpy change associated with the small pressure variation (i.e., $V\Delta P$, $\Delta P < 1$ bar) are negligible compared to the heat effects arising from chemical reactions. A flat SCHF curve is expected in the absence of chemical reactions when only heat content is measured (see, for example, the SCHF curve of H_2O in Figure 1). After the first run, the mixture I system was measured again. The second SCHF curve (curve b in Figure 2) is flat over the whole temperature range, indicating that the heat effect originating from any further chemical reactions is negligible. The mixture I system apparently reached a final state upon initial heating to 89.0 °C such that no significant chemical reactions appear to occur thereafter. We therefore can use the second SCHF curve as a baseline to subtract the contribution of the heat content in the first SCHF curve. The resulting SCHF curve c in Figure 2 shows only the heat effects associated with the chemical reactions during the first heating. The heat thus measured for the SCHF peak(s) is the total enthalpy change (ΔH) of reaction(s). This in turn approximates the enthalpy change at 25 °C, if one neglects the heat capacity change associated with the reaction(s), which is a good approximation. We obtained integral heats of -7.2 ± 0.4 kJ/mol (on a molar formula basis of $5.15Na_2O-1.00Al_2O_3-3.28SiO_2-165H_2O$ of the synthesis system) for the chemical reaction(s) associated

TABLE 1: Chemical Analysis of Solid Samples Collected from the Mixture I Synthesis System

synthesis			solid	chemical analysis of solid product, wt %			
run	t, h[a]	T, °C	weight, g	Na_2O	Al_2O_3	SiO_2	H_2O
A	1.64	34.4	0.465	4.0	5.1	83.8	9.6
B	4.52	51.5	0.762	12.6	19.4	52.2	17.3
C	6.09	60.8	0.803	15.3	25.0	42.4	20.5
D	7.11	66.8	0.760	16.4	26.8	38.2	21.2
E	8.28	73.8	0.765	16.1	26.9	36.6	21.5
F	9.42	80.5	0.793	168	26.6	37.4	22.6
G	9.99	83.9	0.824	16.3	24.3	37.3	25.3
H	10.9	89.0	0.834	16.2	24.8	35.9	25.5
I	13.7[b]	97.2	0.836	15.7	25.7	34.9	25.2

[a] Synthesis time, t, is counted as the scanning time at a heating rate of 0.1 °C/min. There is 1 h between the initial mixing for preparation of the synthesis mixture and the start of scanning. [b] Scanning temperature reached 97.2 °C after 12.2 h of heating and remained isothermal at this temperature for 1.5 h.

TABLE 2: Chemical Analysis of the Solutions in the Mixture I Synthesis System

synthesis				chemical analysis of solution, wt %			
run	t, h[a]	T, °C	solution,[a] g	Na_2O	Al_2O_3	SiO_2	H_2O[b]
A	1.64	34.4	7.04	8.87	2.60	0.248	88.3
B	4.52	51.5	6.74	8.06	0.936	0.290	90.7
C	6.09	60.8	6.70	7.63	0.214	1.31	90.9
D	7.11	66.8	6.74	7.63	0.151	1.92	90.3
E	8.28	73.8	6.74	7.70	0.132	2.13	90.0
F	9.42	80.5	6.71	7.56	0.115	1.80	90.5
G	9.99	83.9	6.68	7.58	0.065	1.78	90.6
H	10.9	89.0	6.67	7.52	0.031	1.71	90.7
I	13.7[b]	97.2	6.66	7.67	0.024	1.75	90.6

[a] As weight difference between the whole mixture (7.50 g) and the solid part (see Table 1). [b] Estimated by mass balance in solutions.

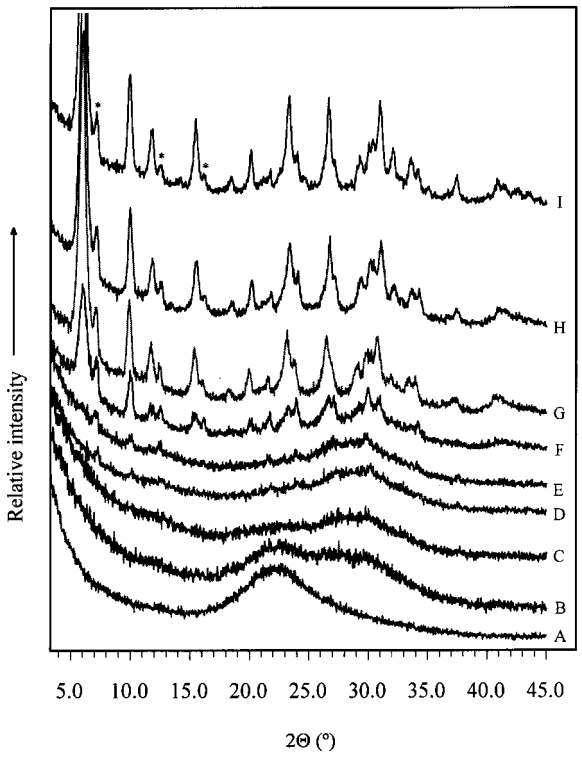

Figure 3. Powder XRD patterns of the solid samples collected after some selected times of reaction of mixture I (see Figure 2).

with the high-temperature peak between 73.8 and 89.0 °C and -95.7 ± 3.0 kJ/mol for those associated with the low-temperature peaks between 34.4 and 73.8 °C. The high-temperature peak is well separated from the low-temperature peaks. The SCHF curve between the high-temperature peak and the low-temperature peaks is near the baseline implying a "standstill" of the chemical reactions during this interval of the synthesis process. The low level of the SCHF curve (curve c in Figure 2) at the early heating period (before heating to 34.4 °C) suggests that the exothermic chemical reactions take place slowly in the low-temperature range (from room temperature to 34.4 °C). Since chemical reactions occurred between the time of the mixing for the preparation of mixture I and the time when the mixture was heated to 34.4 °C in the calorimeter (i.e., 2.4 h later), to a first-order estimate, the extent of the chemical reaction (see the section of chemical analysis) in this period corresponds to −7.8 kJ/mol. This gives an overall enthalpy change of the mixture I synthesis system from the zero-time mixing to the stage at 73.8 °C of -103.5 ± 5.0 kJ/mol.

To ascertain the nature of the chemical reactions associated with the observed SCHF peaks, we performed a series of in situ syntheses and stopped them at various selected temperatures (marked by capital letters in Figure 2). Both solid and liquid samples were collected and examined for the associated structural and compositional changes of the chemical species during the course of synthesis.

Powder XRD Patterns. Powder XRD patterns of the solid products collected at various times show no observable peaks for crystalline phases below 60.8 °C (samples A, B, and C, see Figures 2 and 3). On heating from 34.4 to 60.8 °C, the XRD amorphous maximum of the solid phase (C and D) around $d = 3.95$ Å decreases and at the same time a new amorphous maximum with a lower spacing centered at $d = 3.05$ Å develops. This suggests that the amorphous phase is evolving to a state of higher density prior to the appearance of any long-range-ordered crystalline phase (i.e., prior to there being any crystal sizes larger than 5−10 nm[14,15]).[16] A similar shift in the position of the XRD amorphous maximum was found during room-temperature aging of aluminosilicate gels.[17]

After heating mixture I to 66.8 °C (D), small XRD peaks corresponding to the LTA structure are observed. Upon further heating to 73.8 °C (E), these peaks grow only slightly. Therefore, the major exothermic peaks in the SCHF curve up to 73.8 °C are dominantly related to the precrystallization chemical reactions (see further results). The heat effect in this range is attributed mainly to the short-range rearrangement of the chemical bonds via bond-breaking and bond-making events (on the length scale of no more than 4 unit cells of FAU and LTA structure[14,15,18]).

Substantial growth of the XRD peaks of crystalline phases can be seen only after heating above 73.8 °C (F). A relatively well-crystallized solid product, dominated by FAU plus a small amount of LTA, is formed after heating to 89.0 °C (H). No further change was observed when heating to 97.2 °C and holding at that temperature for 1.5 h (I, see Figures 2 and 3). The exothermic peak between 73.8 and 89.0 °C thus corresponds to crystallization. About 0.84 g of solid product with a composition of $Na_{0.46}Al_{0.46}Si_{0.54}O_2 \cdot 1.29H_2O$ can be obtained from 7.50 g of mixture I (1.18 g/mL). On a TO_2 molar basis of the final zeolite product, the enthalpy change associated with chemical reactions for precrystallization and crystallization are -24.0 ± 1.2 and -1.7 ± 0.1 kJ/mol, respectively. Because the former is 1 order of magnitude more negative than the latter and the formation of the crystalline phase (LTA structure) in the low-temperature region is trivial (Figure 3), the integral ΔH before 73.8 °C (-24.0 ± 1.2 kJ/mol) is an accurate evaluation of the enthalpy change of the precrystallization reactions.

The enthalpy change associated with the initial formation of the amorphous phase from the reactants is an order of magnitude larger than that associated with the crystallization (-24.0 ± 1.2 and -1.7 kJ/mol TO_2, respectively, as directly measured in this study). This is reasonable, since the gelation process involves dissolution of colloidal silica as well as precipitation of a (disordered) tetrahedral framework containing strong Si−O−Si and Si−O−Al bonds from the solution, while crystallization of the gel involves mainly rearrangement of the midrange order (0.5−5 nm) of this framework. Previous studies by high-temperature calorimetry show that the energetic difference between anhydrous aluminosilicate glass and an anhydrous crystalline zeolite phase of the same composition is quite small (often less than 3 kJ/mol TO_2).[19−23] The following reaction sequence illustrates (i) reaction A that corresponds to glass crystallization investigated by high-temperature calorimetry and (ii) reaction B corresponding to the crystallization of gel to zeolite in this study

$$\begin{array}{ccc} \text{Amorphous (anhydrous)} & \xrightarrow{A} & \text{Crystalline (anhydrous)} \\ \downarrow C & & \downarrow D \\ \text{Amorphous (hydrous)} & \xrightarrow{B} & \text{Crystalline (hydrous)} \end{array}$$

It is important to note that the enthalpy change for reaction B (crystallization measured in this work) is small and similar in magnitude to that for reaction A. The similar enthalpy changes for reaction A and B imply that the hydration enthalpies for amorphous phase and crystalline phase (i.e., reactions C and D) are similar. Thus the small enthalpy changes for both reaction A and reaction B suggest that the short-range order strongly influences the energetics of solid phases and the long-range order only weakly influences the energetics.[19−23]

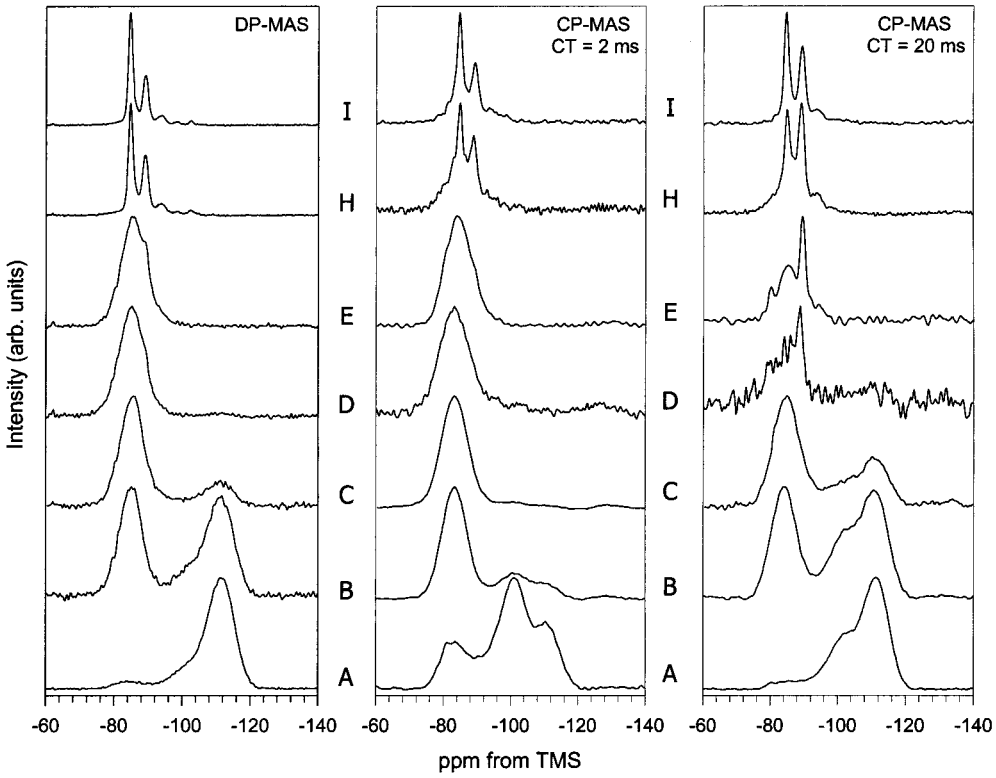

Figure 4. ^{29}Si DP-MAS (left) and CP/MAS NMR spectra at contact times of 2 ms (center) and 20 ms (right) of the solid samples collected after some selected times of reaction of mixture I. Letters refer to sampling times denoted in Figure 2. A 2 ms contact time maximizes signal intensity from the amorphous aluminosilicate precursor, whereas the signal from silica gel and crystalline products increases with contact time owing to longer T_{IS} and ^{1}H $T_{1\rho}$.

Although the energetic difference between the amorphous precursor and the subsequently formed crystalline phase is small, the enthalpy change for the elementary steps of the crystallization reaction such as the incorporation of the dissolved species into zeolite crystals may be much larger. There are slight compositional changes in the solid and the solution, and a change in the degree of hydration during crystallization of the amorphous phase. At present, the contribution to the measured ΔH for crystallization of such changes is not known, but it is presumably small because of the similar solubility of the crystalline phase and the amorphous precursor.

^{29}Si Solid-State NMR. The ^{29}Si MAS NMR spectra of the solid from the early stages in the synthesis (samples A−D) contain broad peaks near −85, −104, and −112 ppm (Figure 4). The peaks at −104 and −112 ppm likely arise from Q^3- and Q^4-type Si in the amorphous silica gel, respectively, based on their chemical shifts and T_{IS} values (1.2 and 17 ms for the peaks at −104 and −112 ppm).[24] CP-MAS spectra taken at short contact times also suggest the presence of a small peak for Q^2-type Si near −95 ppm. Variable-contact-time CP-MAS results indicate that these peaks have similar ^{1}H $T_{1\rho}$'s (20−30 ms), further indicating that they arise from the same phase. The gradual disappearance of these peaks with temperature (A−D) corresponds to dissolution of the colloidal silica. The constant Q^3/Q^4 intensity ratio during this process suggests little structural change in the silica phase. Growth of the peak at −85 ppm can be associated with precipitation of an amorphous aluminosilicate phase. It differs from the silica resonances in being attenuated at long contact times owing to a shorter ^{1}H $T_{1\rho}$ (<10 ms) and shorter T_{IS} (0.9 MS). The position of this peak changes gradually from −84.5 ppm in A to −85.5 ppm in D, consistent with a corresponding increase in the average Si/Al ratio that is also observed from the chemical analyses (see below). For these samples (A−D), the distribution of Si between the amorphous silica and aluminosilicate phases was obtained from least-squares fits of the DP-MAS spectra to a sum of Gaussian curves.

Spectra of sample E contain small (1−3%), narrow peaks at −79.3 and −89.3 ppm, in addition to the broad peak for the amorphous aluminosilicate. Absence of intensity at more negative chemical shifts indicates that dissolution of the colloidal silica is complete at this stage. The peak at −89.3 ppm is consistent with previous reports for Na-LTA-type zeolites and XRD analysis of these samples (Figure 3). That at −79.3 ppm cannot be assigned confidently; the 10 ppm difference from the peak at −89.3 ppm, similar ^{1}H $T_{1\rho}$, and its disappearance upon further crystallization suggest it might arise from Q^3-type defect sites in the LTA phase.

Spectra of samples H and I clearly show five narrow peaks from −84.6 to −102.5 ppm, separated by about 4.4 ppm, due to Si with distinct numbers of Al neighbors ($Q^4(n\text{Al})$, $n = 4-0$[25]) in the crystalline FAU phase that is also apparent in XRD. The Si/Al ratio was calculated from the peak areas assuming no Al−O−Al linkages

$$\text{Si/Al} = \sum_{n=0}^{4} I_n \Big/ \sum_{n=0}^{4} \frac{n}{4} I_n$$

giving 1.22 (±0.04) for both H and I, where I_n *is the integrated intensity of the peak corresponding to Si with n* Al neighbors. The peak areas were obtained from least-squares fits of the DP-MAS spectra to a sum of Gaussian curves and were not corrected for the small amount of LTA phase present, the peak for which overlaps the Q^4(3Al) peak from the FAU phase. Satisfactory fits could only be obtained by including an additional, broad peak. This fitted peak gives a position and width similar to that of the amorphous aluminosilicate and

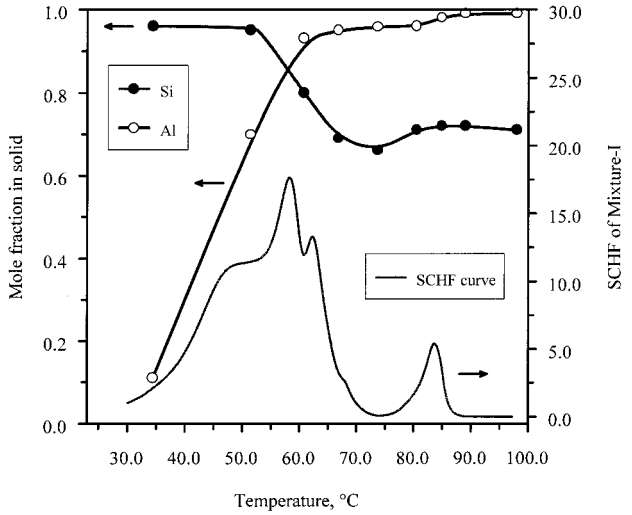

Figure 5. Composition of solid phase in mixture I synthesis as a function of heating temperature. For reference, the SCHF pattern is also shown in the figure.

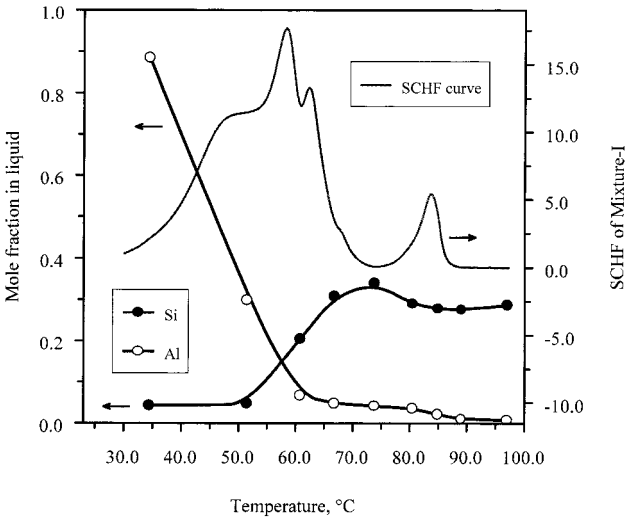

Figure 6. Composition of liquid phase in mixture I synthesis as a function of heating temperature. For reference, the SCHF pattern is also shown in the figure.

accounts for approximately 20% of the spectral intensity. This resonance is more clearly seen in the CP-MAS spectra taken at short contact times. This result suggests that a considerable number of Si sites in the solid occur in poorly ordered regions (such as stacking faults of faujasite layers and surface of fine crystals). Some of these Si sites persist in the synthesis system even after prolonged crystallization under higher temperature (from H to I). These Si sites may represent defects in the fine crystals as indicated by the broadening of XRD peaks (Figure 3) and/or separate amorphous domains trapped inside the aggregates of fine crystals. The presence of these sites may have some bearing on the energetics of the solid phase. However, the effect is expected to be very small because the crystallization enthalpy is only −1.7 kJ/mol (on TO_2 molar basis of the solid product).

Compositional Analysis. Elemental analyses of solid and solution phases are presented in Tables 1 and 2. The Si and Al molar fraction in both phases are plotted against the heating temperature in Figures 5 and 6. The Si/Al ratio and the product of Si and Al concentrations in solution are shown in Figure 7. Combining the Si/Al ratio of the bulk solid phase (measured by elemental analysis) with distribution of Si between the

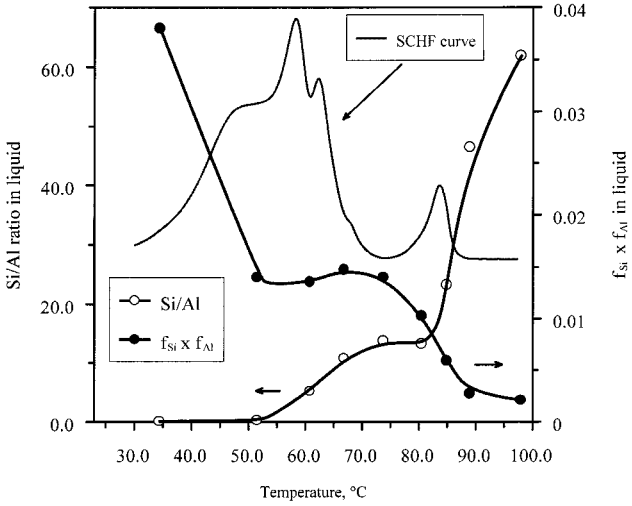

Figure 7. Variation of the compositional characteristics of liquid phase during the mixture I synthesis. For reference, the SCHF pattern is also shown in the figure.

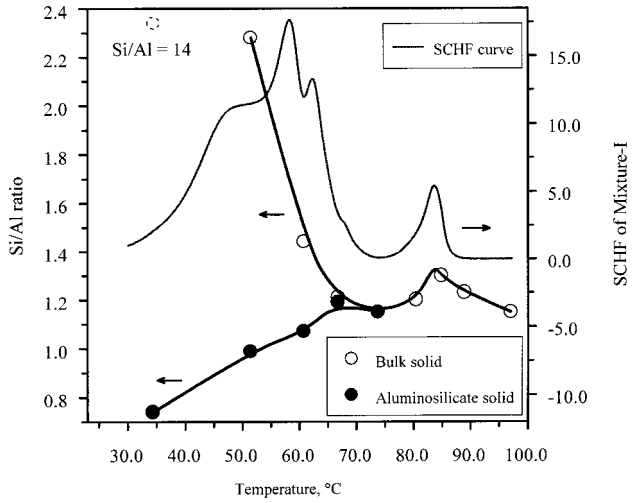

Figure 8. Si/Al ratios of bulk solid and aluminosilicate solid during the mixture I synthesis. For reference, the SCHF pattern is also shown in the figure.

aluminosilicate precursor and in the colloidal silica (measured by ^{29}Si NMR), we estimated the Si/Al ratio of the aluminosilicate precursor in the solid (Figure 8). The slope of the curves between two points in these figures (Figures 5−8) could only be taken as an average rate of the chemical change within the respective period.

Upon initial mixing for the preparation of mixture I, all the Al is present in solution and all of the Si in the solid (colloidal particles). After mixture I is heated to 34.4 °C, about 10% of the total Al was found in the solid and less than 5% of the total Si was present in solution (Figures 5 and 6), suggesting that the extent of chemical reactions (the dissolution of silica and formation of aluminosilicate gel/solid precursor) up to this point (2.4 h after mixing) is small. The low level of the exothermic SCHF curve at 34.4 °C indicates slow chemical reactions, but the reactions could have been faster at the time of the initial mixing.

Upon heating from 34.4 to 51.5 °C, the mole fraction of Al ($f_{Al,L}$) in solution dropped dramatically owing to precipitation of the solid phase (Figure 6). However, the mole fraction of Si ($f_{Si,L}$) in solution remains low and unchanged (Figure 6). The rapid rise of mole fraction of Al in the solid ($f_{Al,S}$) and the persistent low $f_{Si,L}$ in solution strongly imply that the dissolution

rate of colloidal silica is similar to the consumption rate of soluble Si, so that there is no net change of f_{Si} in either the solution or in the solid.[7] The concentration of Si in solution thus appears to be the controlling factor for the rate of formation of the aluminosilicate precursor. The shape of the calorimetric curve in this temperature range (Figure 2) suggests that the chemical reactions speed up quickly to a plateau and remain there for a relatively short period before the next exothermic rise.

Upon heating from 51.5 to 60.8 °C, the $f_{Al,L}$ continues to decrease at the same average rate even though the concentration of Al in solution falls rapidly (Figure 6). At the same time, a gradual increase of $f_{Si,L}$ is seen (Figure 6) and consequently the early dramatic decrease of the $f_{Si,L}f_{Al,L}$ ($T < 51.5$ °C) levels off (Figure 7). The large exothermic peak in the SCHF curve suggests that the involved chemical reactions do not proceed monotonically. Rather, they accelerate to reach a maximum and then slow, implying that a mass-transport limitation may be operative. We note that there is no stirring in the calorimeter. The isothermal condition throughout the calorimetric vessel at any given time (though this temperature increases at the slow heating rate) minimizes convection. Thus this experimental design may accentuate mass-transfer effects associated with depletion or saturation of the aqueous solution.

From 60.8 to 66.8 °C, the $f_{Si,L}$ continues to increase but the $f_{Al,L}$ decreases only slightly (Figure 6). These changes result in an increase of the Si/Al ratio and a nearly constant value of $f_{Si,L}f_{Al,L}$ in solution (Figure 7). Again, an exothermic peak in the calorimetric curve suggests that the depressed chemical reactions are somehow accelerated to reach a new maximum and then depressed again.

During heating from 66.8 to 73.8 °C, the decrease of $f_{Al,L}$ and the increase of $f_{Si,L}$ in solution continue but at slower average rates (Figure 6). The latter seems to reach a maximum at the end of this period when substantial crystallization is just about to begin (see also ref 19). A very small exothermic shoulder in the calorimetric curve indicates another episode of acceleration/depression of the chemical reactions in this period. The depletion of amorphous silica (Figure 4) may be the cause for the quick turn from acceleration to depression this time. It is in this period that the precrystallization reactions come to an end and also a small amount of LTA crystalline phase is observed (Figures 3 and 4). As discussed earlier the crystallization of the minor LTA phase should not contribute significantly to the exothermic curve.

In the final heating stage from 73.8 to 89.0 °C, both the $f_{Al,L}$ and the $f_{Si,L}$ decrease (Figure 6) as shown by the drop of the $f_{Al,L}f_{Si,L}$ in Figure 7. The Si/Al ratio in solution increases dramatically at the end of this period (Figure 7). A similar trend in the Si/Al ratio in solution was reported in the synthesis of low silica zeolite A and high silica zeolite β.[26,27] The Si/Al ratio of the solid changes slightly, and there seems to be a maximum at the time of the SCHF peak for the crystallization (Figure 8). The solution composition changes in this period are consistent with the shift of the dominant phase to be dissolved in the mixture I synthesis from amorphous to crystalline. The latter one has a more stable structure and slightly lower Si/Al ratio; therefore, it is expected to have lower solubility.[28,29]

After heating from 89.0 to 97.2 °C and holding at 97.2 °C for 1.5 h, the already low $f_{Al,L}$ continues to decrease and the $f_{Si,L}$ increases slightly (Figure 6). The drop of the $f_{Al,L}f_{Si,L}$ observed in the previous period levels off (Figure 7). The chemistry of the system has two characteristics in this period: (1) the chemical exchange between solid and solution is governed by a near constant value of the $f_{Al,L}f_{Si,L}$; (2) the direction of the process is to remove Al from solution. Since such a change decreases the entropy of the system ($\Delta S < 0$), the spontaneous chemical reactions must proceed via an energetic driving force ($\Delta H < 0$). The flat SCHF curve suggests little heat effect in this prolonged period, which suggests that the extent of the associated chemical reactions is small. We conclude, therefore, that the chemical reactions proceed at a near equilibrium path (i.e., near zero free energy) and the entropy change must also be very small.

In Situ Calorimetry for Dissolution of Colloidal Silica (Mixture II: $3.88Na_2O-3.28SiO_2-165H_2O$). The SCHF curve of mixture II showed mainly a large exothermic peak in the low-temperature range (27−45 °C, Figure 1). The integral heat released from the system in the temperature range is −39.0 kJ/mol (on molar basis of $3.88Na_2O-3.28SiO_2-165H_2O$ of the system). At the end of the calorimetric measurement, the mixture was a clear solution. The Si species in this silicate solution (Na/Si = 2.4, C_{SiO2} = 0.96) at room temperature are mainly monomers, dimers, and trimer rings.[30] The slight curvature of the SCHF curve of mixture II vs water at the high-temperature range ($T > 45$ °C) may be attributed to the shift of the complex equilibria among the soluble silicate species[31] induced by increasing temperature. The dissolution process is favored by both entropy gain ($\Delta S > 0$ as expected for dissolution) and release of energy ($\Delta H < 0$). The dissolution of silica in the mixture II system is apparently complete when heating to about 45.0 °C, whereas this reaction is significantly slower for the mixture I system (dissolution complete at 73.8 °C). Because the mixing and heating procedure are similar for mixture II and mixture I, the slower rate of dissolution in mixture I, therefore, must be caused by the presence of Al in the system.[7,32]

Before the calorimeter is stabilized to record the SCHF curve (45 min after initial mixing), part of the silica dissolves. Although the completion of the reaction may take 28 h, the initial dissolution rate is very high near room temperature.[7] To estimate the total heat released by dissolution, we performed a new calorimetric measurement by modifying the mixing procedure for preparation of mixture II. The two liquids, colloidal silica suspension and alkali solution, were loaded in two chambers of a specially designed vessel in which the two chambers are connected by a narrow channel (ca. 1 mm diameter, see Figure 9). A viscous gel is formed when the two liquids contact each other. Such a gel (negligible amount) formed in the small channel effectively prevents further mixing and reaction at low temperature. The low level of the SCHF curve in the low-temperature range and the shift of the curve toward the high-temperature range (curve b in Figure 9) are expected for the new mixing procedure for mixture II. The total integral heat, about -90.0 ± 5.0 kJ/mol (on the molar basis of $3.88Na_2O-3.28SiO_2-165H_2O$ of the system) from curve b in Figure 9, can be regarded as a good approximation of the total energy released from the system during dissolution. Because the alkali silicate solution equilibrates rapidly,[30] the speciation of the silicate solution and its energy change are independent of the dissolution history.

In Situ Calorimetry of Zeolite Synthesis Using Silicate Solution as Si Source (Mixture III: $5.15Na_2O-1.00Al_2O_3-3.28SiO_2-165H_2O$). To examine the formation of the aluminosilicate precursor and the subsequent zeolite formation without the complication of silica dissolution, we prepared a gel (mixture III) with the same composition as mixture I and from the same source materials, but the colloidal silica was first dissolved in alkali solution before mixing with aluminate solution. The SCHF

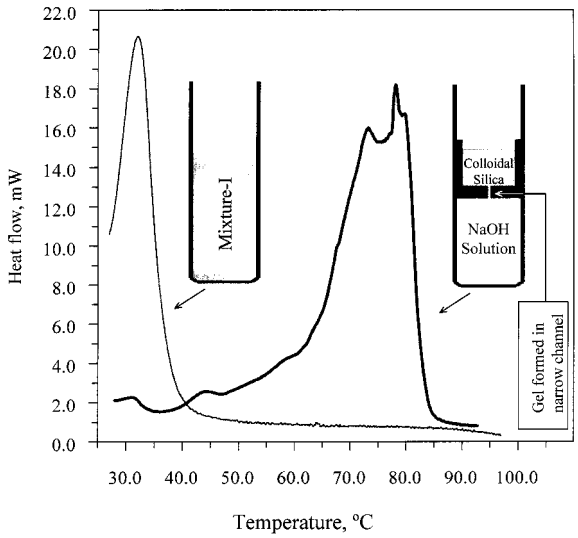

Figure 9. SCHF curves of mixture II ($3.88Na_2O-3.28SiO_2-165H_2O$) and a system of the same overall composition in which NaOH solution and colloidal silica in two chambers are connected by a narrow channel. A negligible amount of a viscous gel formed inside the narrow channel and effectively blocked further reaction between the two liquids in the low-temperature range.

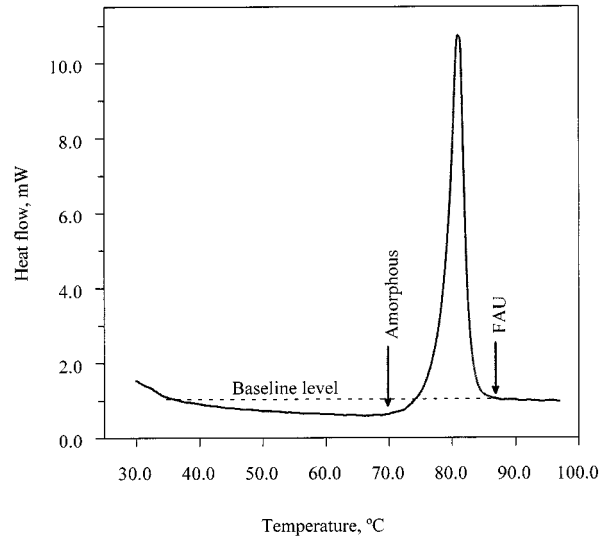

Figure 10. SCHF curve of mixture III ($5.15Na_2O-1.00Al_2O_3-3.28SiO_2-165H_2O$) with silicate solution as silica source. The same weight (7.50 g) of water as that of mixture III was used as reference for calorimetric measurement.

pattern (Figure 10) is distinctly different from that for the mixture I system. First, no major exothermic peaks for the precrystallization chemical reactions in the low-temperature range were observed, indicating that the formation of the aluminosilicate precursor was virtually complete during the initial blending and stirring at room temperature. Second, as the synthesis proceeds from 36.6 to 70.0 °C, the SCHF curve shows a small but gradually increasing endothermic effect (Figure 10). Since the formation of the aluminosilicate precursor is exothermic, the endothermic SCHF curve in this period (Figure 9) suggests that the equilibrium of the digestion reactions, i.e., the reconstruction of the aluminosilicate amorphous gel via dissolution/reprecipitation, gradually shifts toward a higher dissolution with increase of temperature. The dissolution in this period is driven by a positive ΔS, as expected for a dissolution reaction balanced by the positive ΔH. Therefore, it is enhanced by increasing temperature. Third, only the FAU phase but no LTA impurity was detected throughout the synthesis process (Figure 10). The Si/Al ratios of synthetic LTA and FAU are typically 1.0 and 1.1−3.0, respectively. Presumably domains richer in Al (Si/Al = 1) favor the nucleation of LTA over that of FAU. Our results could therefore be rationalized by the absence of microscopic environments (Al-rich aluminosilicate amorphous domains) for nucleation of LTA in the mixture III synthesis. Fourth, the exothermic peak for the crystallization of FAU structure is narrower and corresponds to a slightly lower peak temperature (81.0 °C, see Figure 10) compared to the mixture I synthesis. The relatively sharp peak suggests that crystallization proceeds faster in mixture III than in mixture I. The exothermic heat associated with the crystallization (-2.1 ± 0.1 kJ/mol) for mixture III is slightly greater in magnitude than the corresponding heat (-1.7 ± 0.1 kJ/mol) for the mixture I synthesis. This may be due to a greater extent of dissolution of aluminosilicate precursor and the absence of a minor LTA phase prior to crystallization in contrast to the mixture I synthesis.

Since mixture III and mixture I have the same overall composition, their distinct SCHF curves demonstrate that the nature of the starting materials (corresponding to the different mixing procedure) can significantly impact the precrystallization events. This difference can even affect the later crystallization but to a diminishing degree. One implication of this sensitivity to the nature of the starting materials is that a relatively fast synthesis at low temperature will be more sensitive to the noncompositional synthesis parameters (the nature of the source materials, low-temperature aging, mixing order, stirring, etc.) while a slow synthesis at high temperature will be less sensitive to these factors.

The enthalpy change of the mixture I system in the precrystallization period has been attributed to the dissolution of silica and the formation of the aluminosilicate precursor. The contribution to this enthalpy change by the former reaction can be reasonably estimated by the enthalpy change of the same reaction in mixture II because of the similarity of the mixture I and mixture II systems. This analysis leads to prediction that the formation of aluminosilicate precursor from soluble silicate solution and aluminate solution is slightly exothermic (-2.7 ± 1.7 kJ/mol on TO_2 of zeolite product). Here, the small heat effects of the dilutions were not taken into account.

Mechanistic Implications. Using the scanning calorimetric method, two distinct stages in the zeolite synthesis, precrystallization and crystallization, are observed. In the precrystallization stage, heat is released and an amorphous aluminosilicate precursor is formed. Depending on the nature of the starting materials, the evolution path and ΔH of this stage can vary greatly. When silicate and aluminate solutions are used for preparation of the synthesis mixture (mixture III), rapid formation of aluminosilicate precipitate is not hindered by the dissolution of silica and its associated mass-transport limitation. The amorphous aluminosilicate precursor formed in one step is expected to be relatively uniform in composition. Further homogenization of the amorphous precipitate prior to crystallization may also occur by the digestion reactions when heating the system. Thus the Si/Al value of the microscopic domains is not expected to deviate significantly from their average ratio. During the crystallization period, a small energetic driving force for crystallization was detected, about -2.1 ± 0.1 kJ/mol (on a TO_2 basis of the solid product). The magnitude of the measured enthalpy change is similar to the energetic difference among the different zeolite structures[19−21] and to the difference between anhydrous zeolites and glass of the same composi-

tion,[22,23] which have been directly measured by high-temperature molten oxide solution calorimetry. It should be pointed out that the ΔH measured in this work is the overall enthalpy change of the synthesis system. The entropy change of the synthesis system in the crystallization period should be negative ($\Delta S < 0$) because the product of $f_{Si,L}F_{Al,L}$ in solution is lower after crystallization than before crystallization, and the crystalline phase is more ordered than the amorphous phase. For the spontaneous crystallization reaction to occur, the free energy must be negative ($\Delta G \leq 0$). Given the negative ΔS, the ΔG must be less negative than ΔH. The thermodynamic values of ΔG and ΔS fall into the ranges of -2.1 ± 0.1 to 0 kJ/mol and -7.0 ± 0.4 to 0 J/mol·K respectively (on TO_2 molar basis of the zeolite product) for the crystallization in mixture III.

When the colloidal silica suspension and the aluminate solution were used for synthesis, a uniform mixing of Si and Al can occur only at a length scale greater than the silica particle size (12 nm diameter).[1,7] In the absence of aluminate anions, the dissolution rate of silica in a strongly alkaline solution (pH > 12) is mainly controlled by the surface area of the silica particles and temperature.[7] A comparison of the SCHF curves of mixture II and mixture III (Figures 9 and 10) indicates that under similar conditions the rate for dissolution of silica in the absence of aluminate is considerably slower than that for the formation of the amorphous aluminosilicate precursor. Since the heat released by dissolution of amorphous silica is much greater than that for the formation of the amorphous aluminosilicate precursors, the SCHF curve of mixture I in the precrystallization period can be viewed as dominated by the dissolution of colloidal silica. The dissolution of silica could be inhibited by aluminate anions.[7,32] For example, Iler[32] suggested that adsorption of aluminate anions onto the silica surface inhibits dissolution by electrostatic repulsion of hydroxide ions from the particle surface. Ginter et al.[7] argued that the formation of an insoluble aluminosilicate precipitate is also responsible for the slow rate of silica dissolution in the presence of soluble Al. In this study the SCHF curves not only show the depression of the precrystallization events but also provide direct evidence for a cyclic or oscillatory pattern for the process, which has not been previously reported. Furthermore, the period of each cycle becomes shorter as temperature increases.

The composition of the solution varies continuously during synthesis as indicated by the rapid increase of the Si/Al ratio observed in the solution of the mixture I system (Figure 7). The increase in the Si/Al ratio of the amorphous precursor during the precrystallization period of the mixture I system implies that the amorphous precursors formed at different precrystallization steps have different Si/Al ratios. As compared to the amorphous precursor formed in the mixture III system, the amorphous precursor formed in the mixture I system is expected to have microscopic domains that vary much more from the average Si/Al ratio. The relatively poor microscopic uniformity of the amorphous precursor from mixture I can be attributed to the concurrence of the two precrystallization reactions (the dissolution of silica and the formation of the amorphous precursor) and the influence of the mass-transport limitation. In the mixture III system the two precrystallization reactions are separated (by a different mixing order or equivalently by the different nature of the starting materials), eliminating effects due to dissolution or mass transport.

A specific zeolite structure can be directly synthesized only within a range of the framework Si/Al ratio.[1−4] The Si/Al ratio in the gel places a constraint on the framework Si/Al ratio of the resulting zeolite.[4] The bulk Si/Al ratio of the gels in both mixture I and mixture III synthesis (about 1.2) is near the limiting Si/Al ratio between the FAU and LTA structure.[4,33] Since the nucleation and crystallization of a zeolite can be a local event within the nanometer-sized gel particles,[5] the occurrence of the minor LTA phase from the mixture I system but not from the mixture III system can be understood from the uniformity of the amorphous precursor in terms of Si/Al ratio. The range of Si/Al ratio in the microscopic domains of the amorphous precursor is larger in the mixture I system, making it more likely to contain domains with the low Si/Al ratios that favor the nucleation of the LTA structure.

Conclusions

Scanning microcalorimetry at a slow heating rate is a powerful technique that can be used to track the physicochemical events of zeolite synthesis in both the precrystallization and crystallization periods. Using colloidal silica as the Si source ($5.15Na_2O-1.00Al_2O_3-3.28SiO_2-165H_2O$, mixture I) and a heating rate of 0.10 °C/min for the synthesis of FAU zeolite, the dissolution of silica and the formation of an aluminosilicate amorphous precursor are the primary chemical reactions at low temperatures (<73.8 °C). The former reaction is significantly inhibited owing to the presence of the aluminate anions, although the product of the former reaction (soluble silicate species) is removed by reacting with the aluminate anions. Our calorimetric study provides direct evidence for a cyclic or oscillatory evolution pattern of these precrystallization reactions. The process in this period is associated with a strong energetic driving force. It is controlled not by chemical reactions but by mass-transport limitation of the soluble chemical species. Such an evolution path of mixture I results in a varying Si/Al ratio within the microscopic domains of the aluminosilicate precursor. Using a silicate solution (the dissolved colloidal silica) instead of colloidal silica as the Si source (mixture III, the same composition as mixture I), a rapid mixing of soluble Si and Al species resulted in immediate and one-step formation of an amorphous aluminosilicate precursor with relatively low Si/Al ratio fluctuation in its microscopic domains. For this process the formation of the amorphous precursor was deduced to be exothermic and complete during room-temperature mixing and stirring. A small energetic driving force ($\Delta H = -2.1 \pm 0.1$ kJ/mol, on the TO_2 basis of the crystalline product) for crystallization at 74−89 °C was detected by in situ calorimetry. In addition to the dominant FAU phase, a minor amount of the LTA phase was observed in the mixture I synthesis but not in the mixture III system. The occurrence of the LTA impurity can be attributed to inhomogeneity in the Si/Al ratio of the amorphous aluminosilicate precursor formed the mixture I synthesis.

Acknowledgment. We thank Jean Tangeman, John Neil, and Patrick Piccione for their assistance in preparation of the manuscript. We acknowledge the National Science Foundation for financial support, Grant DMR-97-31782, and the W.M. Keck Foundation for support of the solid-state NMR at UC Davis.

References and Notes

(1) Breck, D. M. *Zeolite Molecular Sieves*; John Wiley: New York, 1974.

(2) Flanigen, E. M. *Adv. Chem. Ser.* **1973**, *121*, 114.

(3) Davis, M. E.; Lobo, R. L. *Chem. Mater.* **1992**, *4*, 756.

(4) Szostak, R. *Molecular Sieves*; Blackie Academic & Professional: New York, 1998.

(5) Mintova, S.; Olson, N. H.; Valtchev, V.; Bein, T. *Science* **1999**, *283*, 958.

(6) de Moor, P.-P. E. A.; Beelen, T. P. M.; van Santen, R. A. *J. Phys. Chem. B* **1999**, *103*, 1639.

(7) Ginter, D. M.; Went, G. T.; Bell, A. T.; Radke, C. J. *Zeolites* **1992**, *12*, 733.

(8) Calvet, E. *Experimental Thermochemistry*; Interscience Publishers Ltd.: London, 1956; p 237.

(9) Hemminger W.; Sarge S. M. *Handbook of Thermal Analysis and Calorimetry, Volume 1, Principles and Practice*; Brown, M. E., Ed.; Elsevier: Amsterdam, 1998; Chapter 1.

(10) Petrova, N.; Kirov, G. N. *Thermochim. Acta* **1995**, *269/270*, 443.

(11) Persson, A. E.; Schoeman, B. J.; Sterte, J.; Otterstedt, J.-E. *Zeolites* **1994**, *14*, 557.

(12) Li, Q.; Creaser, D.; Sterte, J. *Microporous Mesoporous Mater.* **1999**, *31*, 141.

(13) Chase, M. W.; Davies, C. A.; Downey, J. R.; Frurip, D. J.; McDonald, R. A.; Syverud, A. N. *JANAF Thermochemical Tables*, 3rd ed.; *J. Phys. Chem. Ref. Data* **1985**, *14* (Suppl. 1).

(14) Jacobs, P. A.; Derouane, E. G.; Weitkamp, J. *J. Chem. Soc., Chem. Commun.* **1981**, 159.

(15) Roozeboom, F.; Robson, H. E.; Chan, S. S. *Zeolites* **1983**, *3*, 321.

(16) Cullity, B. D. *Elements of X-ray Diffraction*; Addison-Wesley: Reading, MA, 1978; p 321.

(17) Katovic, A.; Subotic, B.; Smit, I.; Despotovic, Lj. A.; Curic, M. *ACS Symp. Ser.* **1989**, *398*, 124.

(18) Meier, W. M.; Olson, D. H.; Baerlocher, Ch. *Atlas of Zeolite Structure Types*; Elsvier: Boston, MA, 1996.

(19) Petrovic, I.; Navrotsky, A.; Davis, M. E.; Zones, S. I. *Chem. Mater.* **1993**, *5*, 1545.

(20) Navrotsky, A.; Petrovic, I.; Hu, Y.; Chen, C.-Y.; Davis, M. E. *J. Non-Cryst. Solids* **1995**, *192*, 474.

(21) Navrotsky, A.; Petrovic, I.; Hu, Y.; Chen, C.-Y.; Davis, M. E. *Microporous Mater.* **1995**, *4*, 95.

(22) Navrotsky, A.; Hon, R.; Weill D. F.; Henry, D. J. *Geochim. Cosmochim. Acta* **1980**, *44*, 1409.

(23) Navrotsky, A.; Peraudeau, G.; McMillan P.; Coutures, J. P. *Geochim. Cosmochim. Acta* **1982**, *46*, 2309.

(24) Maciel, G. E.; Sindorf, D. W. *J. Am. Chem. Soc.* **1980**, *102*, 7607.

(25) Engelhardt Von G.;, Lohse, U.; Lippmaa, E.; Tarmak M.; Mägi, M. *Z. Anorg. Allg. Chem.* **1981**, *482*, 49.

(26) Angell, C. L.; Flank, W. H. *ACS Symp. Ser.* **1977**, *40*, 194.

(27) Perez-Pariente, J.; Martens, J. A.; Jacobs, P. A. *Appl. Catal.* **1987**, *31*, 35.

(28) Zhdanov, S. P. *Adv. Chem. Ser.* **1971**, *101*, 20.

(29) Ejaz, T.; Jones, A. G *J. Chem. Eng. Data* **1999**, *44*, 574.

(30) Engelhardt, G.; Michel, D. *High-Resolution Solid-State NMR of Silicate and Zeolites*; John Wiley & Sons: New York, 1987.

(31) Sefcik, J.; McCormic, A. V. *Ceram. Process.* **1997**, *43*, 2773.

(32) Iler, R. K. *The Chemistry of Silica*; Wiley: New York, 1979.

(33) de Vos Burchart, E.; Jansen, J. C.; van Bekkum, H. *Zeolites* **1989**, *9*, 432.